

Non-watertight Mesh Reconstruction

Partha Ghosh

University of Tübingen

Abstract

Reconstructing 3D non-watertight mesh from an unoriented point cloud is an unexplored area in computer vision and computer graphics. In this project, we tried to tackle this problem by extending the learning-based watertight mesh reconstruction pipeline presented in the paper ‘Shape as Points’. The core of our approach is to cast the problem as a semantic segmentation problem that identifies the region in the 3D volume where the mesh surface lies and extracts out the surfaces from the detected regions. Our approach achieves compelling results compared to the baseline techniques.

Keywords: Surface Reconstruction, Differentiable Rendering

1 Introduction

Reconstructing surfaces from scanned 3D points has been an important research area for several decades. With the wide proliferation of 3D scanners, the problem of surface reconstruction has received significant attention in the graphics and vision communities. In recent years, neural implicit representations gained popularity in 3D reconstruction due to their expressiveness and flexibility. But, the existing works in this area concentrated on the representation and reconstruction of watertight mesh only.

In computer vision and graphics, watertight meshes usually describe meshes consisting of one closed surface. In this sense, watertight meshes do not contain holes and have a clearly defined inside ([David Stutz, 2021](#)). But in reality, most of the objects are not watertight and therefore the reconstruction of the mesh from the point cloud sampled from such objects should also reflect the non-watertightness. But reconstructing non-watertight meshes remained an unexplored area in this domain. Therefore, in this project, we tried to tackle this problem by extending the learning-based 3D watertight mesh reconstruction pipeline presented in the paper ‘Shape as Points’ (SAP) ([Peng et al., 2021](#)).

The existing pipeline in SAP can only be used to reconstruct the watertight mesh from unoriented point cloud even when the point cloud exhibits non-watertightness. Therefore to achieve our goal, it is required to detect and extract out only the relevant part of the watertight mesh defined by the point cloud.

The core of our approach is to cast the problem as a semantic segmentation problem. We take the output representation from the SAP pipeline and apply semantic segmentation to it to identify the region in the 3D volume where the mesh surface lies and then we can extract the non-watertight mesh with the application of marching cube algorithm. The advantage of our approach is its simplicity and robustness. Compared to the hand-engineered filtering techniques that we used as baselines, our method achieves compelling results both qualitatively and quantitatively.

In summary, the main contributions of this work are:

- We present a novel machine learning-based approach for generating high-quality non-watertight meshes.
- We show that our approach achieves significantly better results than the hand-engineered filtering based baseline methods both qualitatively and quantitatively.

We organize the structure of the report as follows. We first provide an overview of the learning-based pipeline in SAP and its limitations in Section 2. We then introduce details of our methodology in Section 3, followed by the description of the baseline methods and the effectiveness of our proposed model compared to the baselines both quantitatively and qualitatively in Section 4.

2 Reviewing SAP

In this section, we briefly review the learning-based watertight surface reconstruction pipeline in SAP (Peng et al., 2021) and analyze the limitation of PSR indicator grid for non-watertight mesh reconstruction.

2.1 Learning-based Watertight Surface Reconstruction

The learning-based watertight surface reconstruction setting in SAP takes a noisy, unoriented point cloud as input and outputs a watertight mesh. More specifically, taking the noisy, unoriented point cloud as input the network predicts a clean oriented point cloud which is then fed into the Differentiable Poisson Solver (Section 2.1.1) to produce an occupancy indicator grid and the watertight mesh is then extracted by running the Marching Cube algorithm on this occupancy indicator grid. The key idea of this work was to introduce differentiability in the classic Poisson Surface Reconstruction algorithm. The model was trained with watertight meshes as ground truth and consequently was supervised directly with the ground truth occupancy grid obtained from these meshes. Figure 1 illustrates the pipeline of the learning-based surface reconstruction task.

2.1.1 Differentiable Poisson Solver

The Differentiable Poisson Solver (Peng et al., 2021) is the differentiable version of the classic Poisson Surface Reconstruction (PSR) algorithm (Kazhdan et al., 2006). The PSR algorithm constructs the characteristic function χ of the solid defined by the oriented point cloud — the

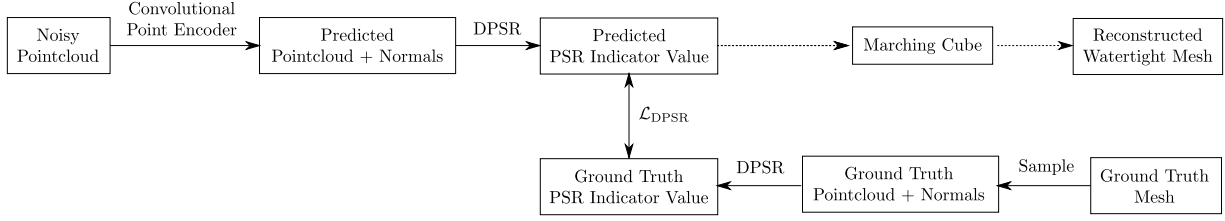


Figure 1: Pipeline for learning-based watertight surface reconstruction in SAP

function whose value is one inside of the solid and zero outside of it — and then extracts the appropriate iso-surface. The characteristic function when realized in the voxel grid, produces the PSR indicator grid.

Let $\mathcal{P} = \{(\mathbf{c}_i, \mathbf{n}_i)\}$ be a set of oriented point cloud sampled from the surface of a solid M , where $\mathbf{c}_i \in \mathbb{R}^3$ denotes a spatial coordinate on the surface of the solid and $\mathbf{n}_i \in \mathbb{R}^3$ is its corresponding surface normal. Let $\chi : \mathbb{R}^3 \rightarrow \mathbb{R}$ be the characteristic function. Then, the Divergence theorem states that

$$\iiint_M (\Delta \cdot \chi) dV = \iint_{\partial M} (\nabla \chi \cdot \mathbf{n}) dS.$$

Approximating the right hand side of the above equation with the given samples gives rise to the Poisson equation as follows:

$$\Delta \chi = \nabla \cdot \mathbf{v}$$

where, $\mathbf{v}(\mathbf{x}) = \sum_{(\mathbf{c}_i, \mathbf{n}_i) \in \mathcal{P}} \delta(\mathbf{x} - \mathbf{c}_i) \mathbf{n}_i$ where δ is the Kronecker delta. Solving this set of linear Partial Differential Equations (PDEs) differentiably, involves discretizing the point normal field \mathbf{v} uniformly by rasterizing the point normals onto a uniformly sampled voxel grid. The differentiability in the point rasterization process comes via inverse trilinear interpolation. With Spectral methods, the original signal can be decomposed into a linear sum of sine/cosine basis functions whose derivatives can be computed analytically. Therefore, employing this method one can first solve for the unnormalized characteristic function χ' without the boundary conditions

$$\chi' = \text{IFFT}(\tilde{X}), \quad \tilde{X} = \tilde{g}_{\sigma,r}(\mathbf{u}) \odot \frac{i\mathbf{u} \cdot \tilde{\mathbf{v}}}{-2\pi \|\mathbf{u}\|^2}, \quad \tilde{g}_{\sigma,r}(\mathbf{u}) = \exp\left(-\frac{2\sigma^2 \|\mathbf{u}\|^2}{r^2}\right)$$

where the Fast Fourier Transform of \mathbf{v} is denoted as $\tilde{\mathbf{v}} = \text{FFT}(\mathbf{v})$; $\mathbf{u} := (u, v, w) \in \mathbb{R}^{n \times d}$ denotes the spectral frequencies corresponding to the (x, y, z) spatial dimensions and $\text{IFFT}(\tilde{\chi})$ represents the Inverse Fast Fourier Transform of $\tilde{\chi}$. $\tilde{g}_{\sigma,r}(\mathbf{u})$ is a Gaussian smoothing kernel of bandwidth σ at grid resolution r in the spectral domain to mitigate ringing effects as a result of the Gibbs phenomenon from rasterizing the point normals. Therefore the normalized differentiable characteristic function is given by

$$\chi = \frac{m}{\text{abs}(\chi'|_{\mathbf{x}=0})} \left(\chi' - \frac{1}{|\{\mathbf{c}_i\}|} \sum_{\mathbf{c} \in \{\mathbf{c}_i\}} \chi'|_{\mathbf{x}=\mathbf{c}} \right).$$

2.1.2 Architecture

The very first component of the learning based pipeline is the convolutional point encoder network as proposed in (Peng et al., 2020). This network encode the noisy unoriented point cloud coordinates $\{\mathbf{c}_i\}$ into a feature ϕ_θ encapsulating both local and global information about the input point cloud. Here, θ refers to network parameters.

Let $\phi_\theta(\mathbf{c})$ denote the feature at any particular point \mathbf{c} obtained from feature volume ϕ_θ using trilinear interpolation. Then given the feature $\phi_\theta(\mathbf{c})$ a shallow Multi-Layer Perceptron (MLP) \mathbf{f}_θ predict k -offsets for \mathbf{c} :

$$\Delta\mathbf{c} = \mathbf{f}_\theta(\mathbf{c}, \phi_\theta(\mathbf{c}))$$

Therefore we get the updated point positions $\hat{\mathbf{c}}$ by adding the offsets $\Delta\mathbf{c}$ to the input point position \mathbf{c} . These additional offsets densify the point cloud, leading to enhanced reconstruction quality. Following the authors, we also conducted all our subsequent experiments with $k = 7$.

Given the updated points $\hat{\mathbf{c}}$ a second MLP \mathbf{g}_θ is trained to predict the corresponding normals:

$$\hat{\mathbf{n}} = \mathbf{g}_\theta(\hat{\mathbf{c}}, \phi_\theta(\hat{\mathbf{c}})).$$

The same decoder architecture as in (Peng et al., 2020) is used for both \mathbf{f}_θ and \mathbf{g}_θ . The network comprises 5 layers of ResNet blocks with a hidden dimension of 32.

2.1.3 Training and Inference

The authors used watertight and noise-free meshes for supervision and acquire the ground truth indicator grid by running PSR algorithm (Kazhdan et al., 2006) on a densely sampled point clouds of the ground truth meshes with the corresponding ground truth normals. Mean Square Error (MSE) loss on the predicted ($\hat{\chi}$) and ground truth (χ) indicator grid

$$\mathcal{L}_{\text{DPSR}} = \|\hat{\chi} - \chi\|^2$$

is used for training the model with a learning rate of 5e-4. During inference, the trained model predicts the normals and offsets and then DPSR solves for the PSR indicator grid, and after that Marching Cubes (Lorensen and Cline, 1987a) extract meshes from the PSR indicator grid as demonstrated in Figure 1.

2.2 Limitation of the Learning-based Pipeline in SAP

The limitation of the learning-based pipeline, for non-watertight mesh reconstruction comes from the PSR algorithm itself.

By definition, the characteristic function relies on the assumption that a solid object has an interior and an exterior part with an enclosed boundary. In practice, deriving the functional form of the boundary of a solid is very difficult and using it to solve for the characteristic function is impractical. Thus, we resort to using the point cloud sampled from the surface of the solid and solve the Poisson equation to get the PSR indicator grid. But by using point cloud,

we no longer have an enclosed boundary but many tiny holes where no samples are present. In these regions where no samples are present the indicator values diffuse from 1 to 0 gradually rather than a sharp change. This problem can be partially mitigated in SAP by densifying the point cloud by predicting offsets.

This problem is more pronounced in the case of non-watertight mesh reconstruction since the regions where there are no samples are much larger. Therefore, running the PSR algorithm on a point cloud sampled from a non-watertight mesh results in a PSR indicator grid where a sharp transition from 1 to 0 can be observed where there are samples (sharpness depends on the point cloud density at that region) and regions where there are no samples, indicator values gradually diffuse from 1 to 0. Therefore running Marching Cube algorithm on this PSR grid results in a watertight mesh where reconstructed surfaces are well constructed and match with the boundaries defined by the samples but also produces excess surfaces of arbitrary topology where there are no samples.

In this project, we tried to mitigate this problem by identifying the regions with a sharp transition from 1 to 0 in the PSR grid.

3 Our Approach

Given a noisy, unoriented point cloud in \mathbb{R}^3 our goal is to reconstruct a surface (watertight or non-watertight) that fits the point cloud. We do this by extending the existing learning-based watertight surface reconstruction pipeline in SAP (Peng et al., 2021) with a Surface Mask Prediction Network.

3.1 Method

To begin with, we define “A Surface Mask” of an object surface to be a volume in the 3D space that encapsulates the object surface. Given a PSR indicator grid, our objective is to predict a surface mask such that it only encapsulates the actual object surface and does not encapsulate other non-surface region. Thus, our surface mask has to be thick enough such that it captures the actual surface entirely and thin enough such that it does not capture any non-surface region. The reason behind this approach is that once we can generate the appropriate surface mask, we can run the marching cube algorithm restricted to the masked region and therefore we can extract only the relevant object surface.

To achieve this we observed that, the PSR indicator grid constructed from a point cloud sampled from a non-watertight mesh shows a sharp change in the gradient where there are point samples, whereas the gradient changes slowly where there are no samples. But the sharpness of the gradient change depends on the density of the point cloud in that region. Therefore, simple hand-engineered gradient-based filtering is not sufficient to detect the regions (See the comparisons below in Section 4.3). Thus, we resort to Machine Learning based approach.

Surface Mask Prediction Network

We can regard the aforementioned problem as a semantic segmentation problem in 3D as we want to label each voxel if it belongs in the surface mask region and thus provides a dense 3D surface mask. Now the surface mask is a local feature of the PSR indicator grid and requires a small receptive field to label a voxel by identifying whether a sharp gradient change occurs in the vicinity of the voxel. Therefore a standard 3D U-NET, with one input and output channel, is sufficient to predict the surface mask.

Following the work on 3D U-NET (Özgün Çiçek et al., 2016), in the analysis part, we used at each stage a **DoubleConv** module consists of two $3 \times 3 \times 3$ convolutions each followed by batch normalization and a rectified linear unit (ReLU) and then a $2 \times 2 \times 2$ max-pooling with a stride of two in each dimension. In the synthesis part, we used 3D transposed convolution operator (Zeiler et al., 2010) each followed by the **DoubleConv** module. We also used skip-connections to fuse high-resolution features from the analysis path into the synthesis path. We call this network “Surface Mask Prediction Network” (SMPN). The illustration of the network is given in Figure 2.

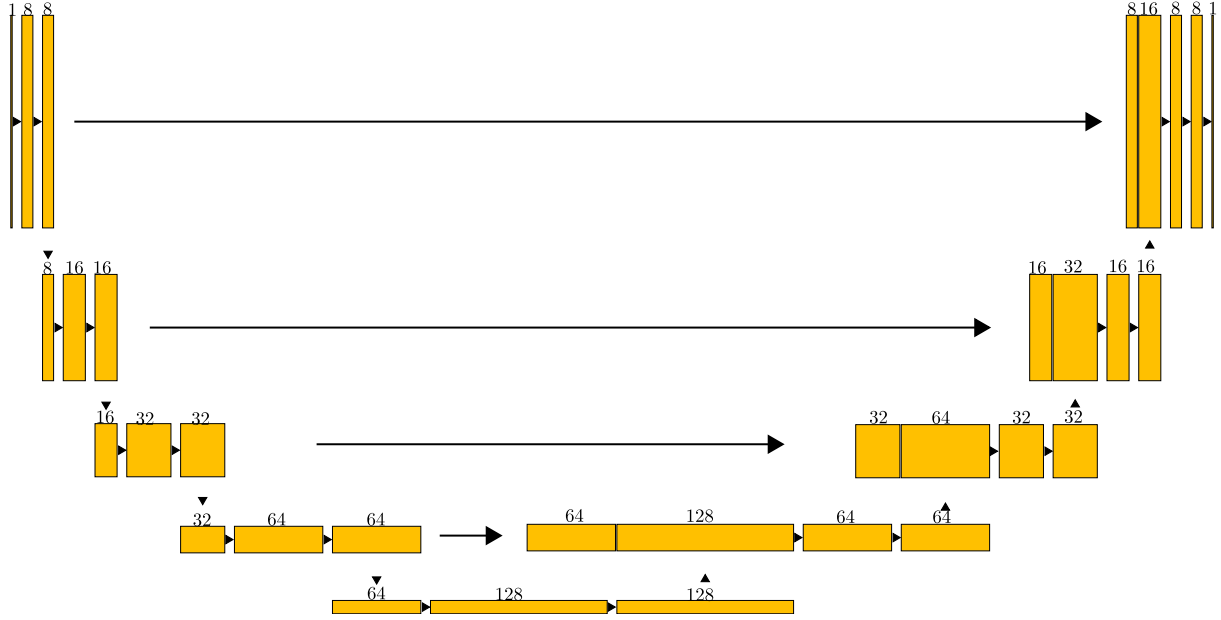


Figure 2: Model architecture of the Surface Mask Prediction. A standard 3D U-NET architecture with feature channels 8, 16, 32, 64, 128.

Now with the SMPN, we can extend the learning-based watertight surface reconstruction pipeline as illustrated in Figure 3 to facilitate non-watertight surface reconstruction.

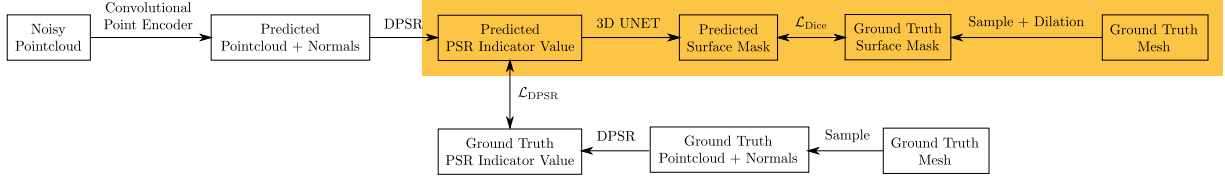


Figure 3: Schematic view of the extended SAP pipeline. The highlighted portion indicates the extension.

3.2 Implementation Details

3.2.1 Dataset

We generate our training data using the watertight meshes from ShapeNet (Chang et al., 2015) dataset. For all our experiments we used the meshes of the following classes — Box, Car, Chair, Ship, and Sofa.

3.2.2 Data Preprocessing Pipeline

Given a watertight mesh from ShapeNet dataset (Chang et al., 2015), We first apply a random rotation to the mesh and then we translate and scale it to fit into the $[0, 1]^3$ unit cube. We then use this transformed mesh to densely sample oriented points and feed them to the PSR algorithm (Kazhdan et al., 2006) to generate the ground truth PSR indicator grid. From this point cloud, we then remove points that fall within some randomly selected regions, which we use as the ground truth point cloud. We then scale this ground truth point cloud and discretize it to create the voxel grid and apply a $7 \times 7 \times 7$ 3D dilation kernel on this voxel grid to generate the ground truth surface mask.

3.2.3 Training and Inference

During the training phase, we train both the learning-based watertight surface reconstruction pipeline and the surface mask prediction network jointly. We first obtain the predicted PSR indicator grid $\hat{\chi}$ by feeding the unoriented point cloud $\hat{\mathbf{c}}$ as input to the learning-based pipeline in SAP and then use the predicted PSR indicator grid $\hat{\chi}$ as input to our Surface Mask Prediction Network to generate the surface mask \hat{M} . The corresponding ground truth mask M is obtained as described in Section 3.2.2. To compute the loss between the predicted and the ground truth mask, we used the dice loss (Milletari et al., 2016)

$$\mathcal{L}_{\text{Dice}} = 1 - \frac{2 \sum_{i,j,k} M_{ijk} \hat{M}_{ijk} + 1}{\sum_{i,j,k} M_{ijk}^2 + \sum_{i,j,k} \hat{M}_{ijk}^2 + 1}$$

which considers the loss information both locally and globally as it is critical to predict a precise surface mask. Also to train the SAP pipeline we use the same $\mathcal{L}_{\text{DPSR}}$ loss as discussed in Section 2.1.3. Thus to train both the networks jointly, we used the following total loss

$$\mathcal{L} = \mathcal{L}_{\text{DPSR}} + \mathcal{L}_{\text{Dice}}.$$

We implement all models in PyTorch (Paszke et al., 2019) and for training, we use the Adam optimizer (Kingma and Ba, 2014) with a learning rate of 5e-4 and batch size of 16. We trained the models using NVIDIA GeForce RTX 3090.

During inference, given any input point cloud, we first use the learning-based watertight surface reconstruction pipeline in SAP to predict the PSR indicator grid and use the predicted indicator grid as input to our surface mask prediction network to predict the surface mask and run Marching Cubes (Lorensen and Cline, 1987b) on the indicator grid restricted to the surface mask region to extract the non-watertight mesh. Figure 4 illustrates the inference mechanism.

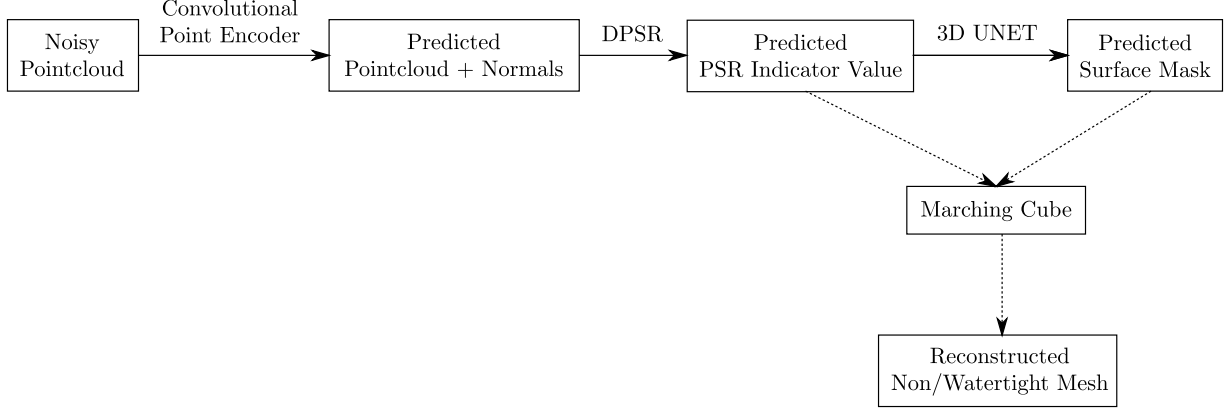


Figure 4: Schematic view of the inference mechanism

4 Experimental Results

4.1 Evaluation Metrics

We considered Chamfer Distance and Hausdorff Distance as our evaluation metrics. Given two point clouds S_1 and S_2 , the Chamfer Distance (CD) and Hausdorff Distance (HD) is defined as follows

$$CD(S_1, S_2) = \frac{1}{|S_1|} \sum_{x \in S_1} \min_{y \in S_2} \|x - y\|_2^2 + \frac{1}{|S_2|} \sum_{x \in S_2} \min_{y \in S_1} \|x - y\|_2^2,$$

$$HD(S_1, S_2) = \max \left\{ \sup_{x \in S_1} \inf_{y \in S_2} \|x - y\|, \sup_{y \in S_2} \inf_{x \in S_1} \|x - y\| \right\}.$$

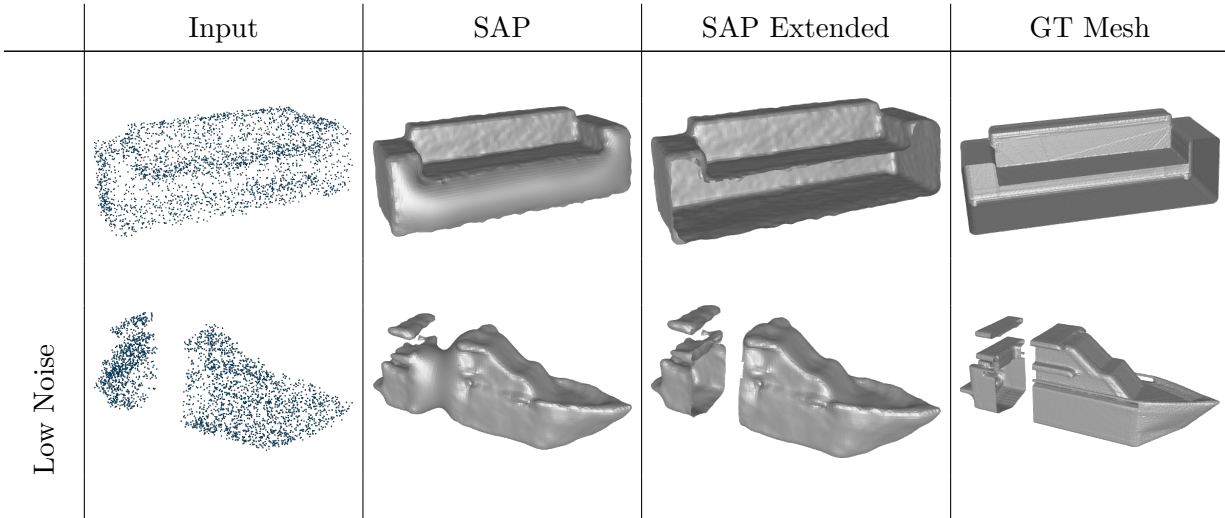
These metrics may not be the best indicator of similarity between two non-watertight meshes since if one of the non-watertight meshes have some tiny holes and the other does not, then this discrepancy may not get reflected in the metric score as we are calculating the metric only with a number of points sampled from the surface of the meshes. Therefore, we also use visual aid for our assessment.


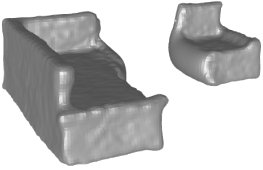
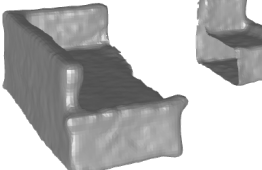
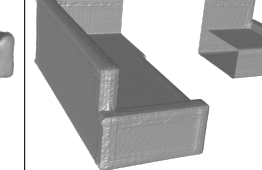
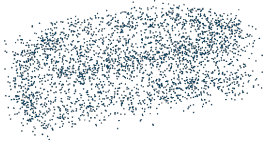
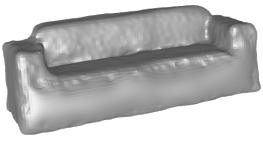
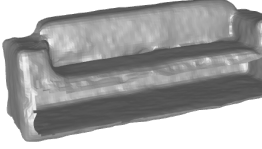
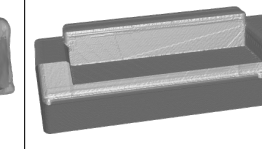
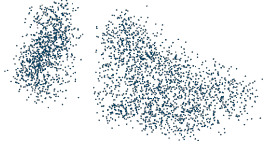
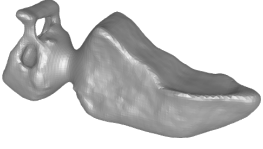
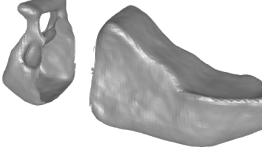
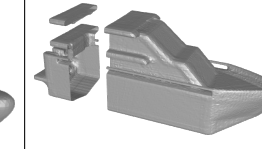
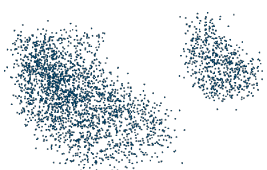
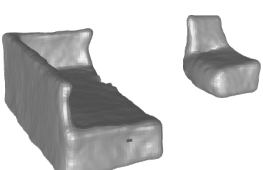
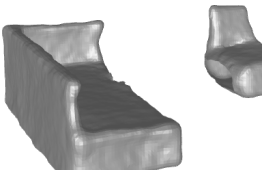
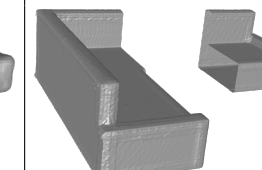
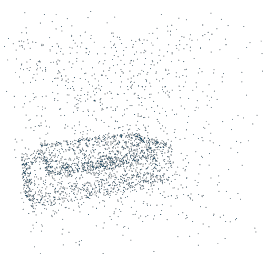
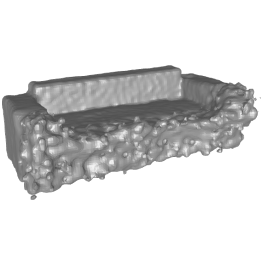
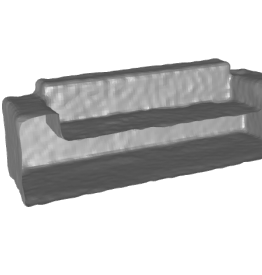
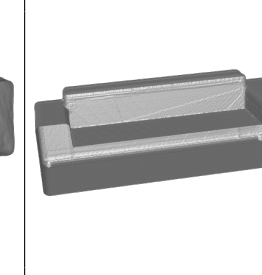
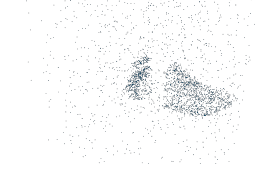
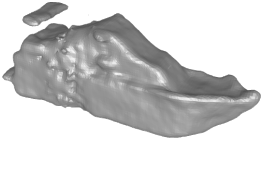
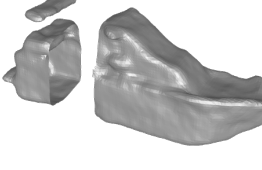
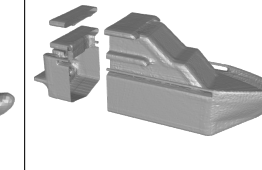
4.2 Non-watertight Surface Reconstruction

In this part, we investigate whether our extension to the SAP pipeline can be used for non-watertight surface reconstruction from unoriented point clouds. We evaluate our method on the single object reconstruction task using noise and outlier-augmented point clouds from ShapeNet as input to our method. We investigate the performance for three different noise levels: (a) Gaussian noise with zero mean and standard deviation 0.005, (b) Gaussian noise with zero mean and standard deviation 0.025, (c) 50% points have the same noise as in a) and the other 50% points are outliers uniformly sampled inside the unit cube. Table 1 shows that our method achieves better results compared to the base SAP pipeline. Also, we can observe that training the entire extended pipeline performs better than training only the SMPN with the backbone frozen. Table 2 shows qualitatively that our method works well with various noise levels augmented in the input point cloud.

Pipeline	Chamfer Distance (\downarrow)	Hausdorff Distance (\downarrow)
SAP	0.009798	0.254690
SAP(freezed) + SMPN	0.000615	0.108691
SAP + SMPN	0.000239	0.071070

Table 1: Quantitative comparison of the performances of the extended pipeline (2nd and 3rd row) with the base pipeline (1st row) on the ShapeNet dataset (mean over 5 classes).



				
High Noise				
				
				
Outliers				
				

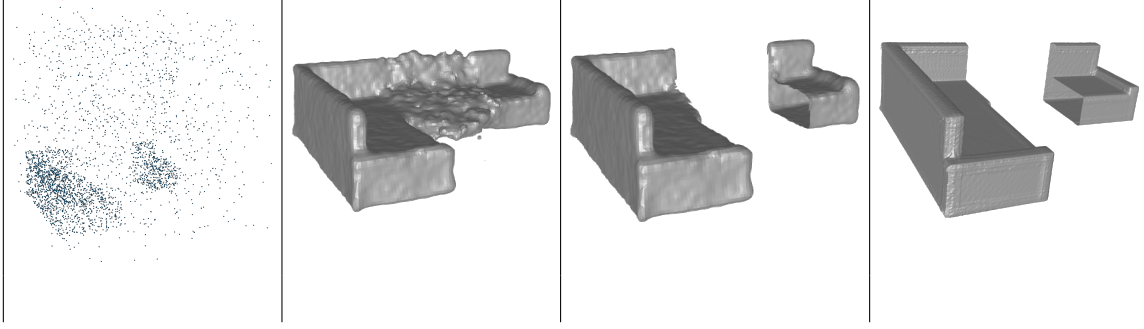


Table 2: Qualitative comparison of the performances of the extended pipeline with the base pipeline in 3 different types of input.

4.3 Comparisons to the Baselines Methods

For baselines, we used the classic Laplacian filter on the PSR indicator grid with various thresholds for mask generation. We first discuss the baseline method with 2D Laplacian filtering. Given a 3D PSR indicator grid, we take each 2D slice and convolve it using a 2D 3×3 Laplace kernel:

$$\begin{bmatrix} 0 & -1 & 0 \\ -1 & 4 & -1 \\ 0 & -1 & 0 \end{bmatrix},$$

to get a silhouette of the edges defined by the indicator grid in that slice. Then we compute the absolute values of the convolved grid and use different thresholds to classify whether a pixel is an actual point on the surface of the mesh. Then, we apply a 7×7 dilation kernel to generate the surface mask and use it together with the PSR indicator grid to extract the non-watertight surface using Marching Cube algorithm.

The baseline method for 3D Laplacian filter is similar as the 2D baseline. In this case, we use a 3D $3 \times 3 \times 3$ Laplace kernel K given by

$$K_1 = \begin{bmatrix} 0 & 0 & 0 \\ 0 & 1 & 0 \\ 0 & 0 & 0 \end{bmatrix}, \quad K_2 = \begin{bmatrix} 0 & 1 & 0 \\ 1 & -6 & 1 \\ 0 & 1 & 0 \end{bmatrix}, \quad K_3 = \begin{bmatrix} 0 & 0 & 0 \\ 0 & 1 & 0 \\ 0 & 0 & 0 \end{bmatrix},$$

where K_i denotes the i -th plane and we use this kernel to convolve the entire grid. Then we compute the absolute values of convolved grid and use thresholding as above and convolve it using a $7 \times 7 \times 7$ dilation kernel to generate the surface mask.

Table 3 and Table 4 show the quantitative and qualitative comparisons respectively. We can observe that the baseline methods do not perform well. Also, a considerable output depends on

the threshold and varies from input to input. Compared to the baseline methods, our method achieves superior performance.

Method	Threshold	Chamfer Distance (\downarrow)	Hausdorff Distance (\downarrow)
2D Laplacian	0.00	0.009798	0.254690
	0.05	0.008534	0.254473
	0.10	0.009470	0.254429
	0.20	0.016016	0.260365
	0.40	0.059645	0.340960
3D Laplacian	0.00	0.009799	0.254690
	0.05	0.008783	0.254579
	0.10	0.010009	0.254576
	0.20	0.023703	0.255712
	0.40	0.088625	0.400718
Ours	-	0.000239	0.071070

Table 3: Quantitative comparison of the performances of the extended pipeline with the baseline methods on the ShapeNet dataset (mean over 5 classes). The table shows performances of the kernel methods (2D/3D Laplacian) for mask generation at various thresholds.

4.4 Ablation Studies

In this section, we investigate the influence of different dilation kernels on the surface mask. We conduct our ablation experiments on ShapeNet for the first setup i.e. with small induced noise (otherwise metric calculation would be inconclusive). We generate our training data with dilation kernels of various widths. We keep the Surface Mask Prediction Network and the SAP pipeline fixed with their optimal configurations. We then train the model with training data generated with a particular dilation kernel and then measured its performance. Table 5 reports the results.

Metric \ Kernel Width				
	3	5	7	9
Chamfer Distance	0.000172	0.000174	0.000221	0.000263
Hausdorff Distance	0.047733	0.042084	0.060259	0.058211

Table 5: Ablation study over kernel width

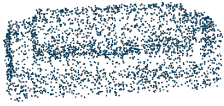
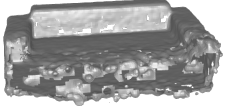
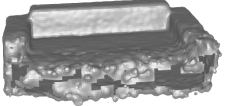
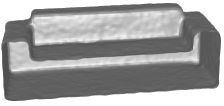
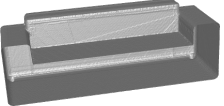
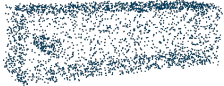





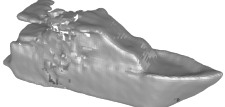
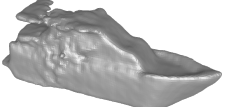
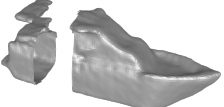
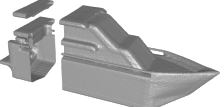
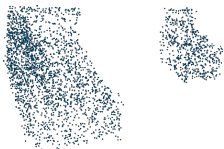
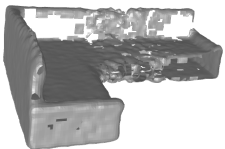
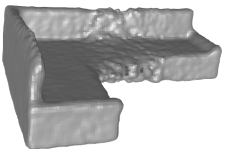
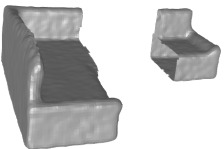
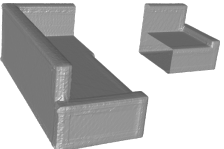
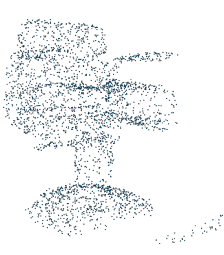
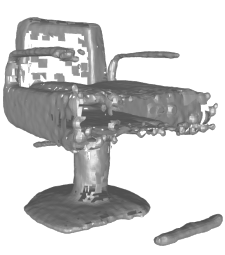
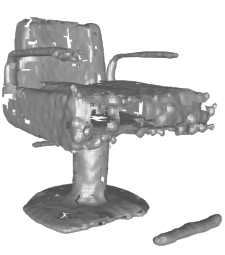
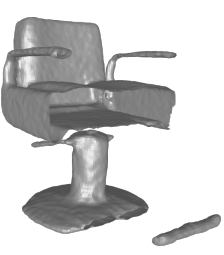

Input	2D Laplacian (with best threshold)	3D Laplacian (with best threshold)	SAP Extended	Ground Truth
				
				
				
				
				

Table 4: Qualitative comparison of the performances of the extended pipeline with the baseline methods (with the best threshold for mask generation) on the ShapeNet dataset.

As we have pointed out before (in Section 4.1), even though the metric shows better performance with kernel width 3, it is not an accurate assessment. We found that the predicted mesh contains very tiny holes at undesired places as being very thin, and the predicted surface mask could not capture the regions where the surface lies very accurately. On the other hand, we notice that training data generated with kernel width 5 gives the best prediction performance both qualitatively and quantitatively.

5 Conclusion

In this project, we have presented a novel method for non-watertight mesh reconstruction performing semantic segmentation on the PSR indicator grid. We demonstrate its effectiveness in reconstructing the non-watertight mesh, compared to the filtering-based baseline methods, both quantitatively and qualitatively.

Limitations. The main limitation of our approach is the usage of dilation kernels to generate the ground truth surface mask. Therefore, it will be interesting to study if there is any way to predict the surface mask without the supervised training. Secondly, our experiments were restricted to reconstructing a single object surface. But we believe that our method can be extended to reconstruct large scenes by combining small non-watertight surface patches, reconstructed in a sliding-window manner. Finally, our initial approach is not end-to-end. Therefore, taking supervision directly from the non-watertight mesh via chamfer loss can be an interesting end-to-end approach to consider for future studies.

6 Acknowledgements

I want to thank Songyou Peng and Chiyu ‘Max’ Jiang for supervising the project and providing me with the necessary guidance and valuable support throughout this research project. I want to thank Prof. Andreas Geiger for the helpful discussions. Also, I want to thank Songyou Peng and Madhav Iyengar for proofreading the report.

References

- David Stutz. A formal definition of watertight meshes, 2021. URL <https://davidstutz.de/a-formal-definition-of-watertight-meshes>. [Online; accessed 17-May-2022].
- Songyou Peng, Chiyu “Max” Jiang, Yiyi Liao, Michael Niemeyer, Marc Pollefeys, and Andreas Geiger. Shape as points: A differentiable poisson solver, 2021.
- Michael Kazhdan, Matthew Bolitho, and Hugues Hoppe. Poisson surface reconstruction, 2006.
- Songyou Peng, Michael Niemeyer, Lars Mescheder, Marc Pollefeys, and Andreas Geiger. Convolutional occupancy networks. In *Computer Vision – ECCV 2020*, pages 523–540. Springer International Publishing, 2020. doi: 10.1007/978-3-030-58580-8_31.

- William E. Lorensen and Harvey E. Cline. Marching cubes: A high resolution 3d surface construction algorithm. *SIGGRAPH Comput. Graph.*, 21(4):163–169, aug 1987a. ISSN 0097-8930. doi: 10.1145/37402.37422. URL <https://doi.org/10.1145/37402.37422>.
- Özgün Çiçek, Ahmed Abdulkadir, Soeren S. Lienkamp, Thomas Brox, and Olaf Ronneberger. 3d u-net: Learning dense volumetric segmentation from sparse annotation. June 2016.
- Matthew D. Zeiler, Dilip Krishnan, Graham W. Taylor, and Rob Fergus. Deconvolutional networks. In *2010 IEEE Computer Society Conference on Computer Vision and Pattern Recognition*. IEEE, jun 2010. doi: 10.1109/cvpr.2010.5539957.
- Angel X. Chang, Thomas Funkhouser, Leonidas Guibas, Pat Hanrahan, Qixing Huang, Zimo Li, Silvio Savarese, Manolis Savva, Shuran Song, Hao Su, Jianxiong Xiao, Li Yi, and Fisher Yu. Shapenet: An information-rich 3d model repository. December 2015.
- Fausto Milletari, Nassir Navab, and Seyed-Ahmad Ahmadi. V-net: Fully convolutional neural networks for volumetric medical image segmentation. June 2016.
- Adam Paszke, Sam Gross, Francisco Massa, Adam Lerer, James Bradbury, Gregory Chanan, Trevor Killeen, Zeming Lin, Natalia Gimelshein, Luca Antiga, Alban Desmaison, Andreas Kopf, Edward Yang, Zachary DeVito, Martin Raison, Alykhan Tejani, Sasank Chilamkurthy, Benoit Steiner, Lu Fang, Junjie Bai, and Soumith Chintala. Pytorch: An imperative style, high-performance deep learning library. In H. Wallach, H. Larochelle, A. Beygelzimer, F. d'Alché-Buc, E. Fox, and R. Garnett, editors, *Advances in Neural Information Processing Systems 32*, pages 8024–8035. Curran Associates, Inc., 2019. URL <http://papers.neurips.cc/paper/9015-pytorch-an-imperative-style-high-performance-deep-learning-library.pdf>.
- Diederik P. Kingma and Jimmy Ba. Adam: A method for stochastic optimization, 2014. URL <https://arxiv.org/abs/1412.6980>.
- William E. Lorensen and Harvey E. Cline. Marching cubes: A high resolution 3d surface construction algorithm. In *Proceedings of the 14th annual conference on Computer graphics and interactive techniques - SIGGRAPH '87*. ACM Press, 1987b. doi: 10.1145/37401.37422.